Vortices in layered superconductors with Josephson coupling

L. N. Bulaevskii, M. Ledvij,* and V. G. Kogan
Ames Laboratory and Department of Physics, Iowa State University, Ames, Iowa 50011
(Received 13 November 1991)

Strongly anisotropic layered superconductors are considered within the Lawrence-Doniach model. The differential finite-difference sine-Gordon equation is derived for the order-parameter phase differences; boundary conditions are formulated for a vortex lattice. The structure of a tilted vortex is considered. The line energy of a single tilted vortex and the free energy of a tilted vortex lattice in moderate magnetic fields are calculated. Deviations from the three-dimensional London theory are substantial for field orientations close to the layers. As the applied field approaches the ab plane, the orientational lock-in transition (tilted-parallel lattice) occurs provided $\lambda_J \lesssim \lambda_{ab}$; here $\lambda_J = \gamma s$ is the Josephson length, γ is the anisotropy parameter, and s is the interlayer spacing. If $\lambda_J \gtrsim \lambda_{ab}$, the tilted lattice transforms first into a new type of vortex arrangement that consists of sets of coexisting parallel and perpendicular vortices (combined lattice). Then, as the field further approaches the ab plane, the combined lattice goes over to the parallel one. The angular dependence of the torque is evaluated for tilted, combined, and parallel lattices, which allows one to experimentally distinguish these phases.

I. INTRODUCTION

Magnetic structure of vortices and vortex lattices in strongly anisotropic superconductors (for example, $NbSe_2$ or high-temperature superconductors, HTSC) is still the subject of intensive discussion. There are few distinct approaches to the problem. The simplest conceptually is the three-dimensional (3D) London theory,[1–5] which simply introduces a tensor in place of the squared penetration depth of the isotropic London theory. The London theory works well in describing magnetic properties of uniform bulk materials provided the penetration depth $\lambda \gg \xi$, the coherence length, and ξ is much larger than the scale of intrinsic inhomogeneities. In layered materials, this scale is the interlayer spacing s, which, therefore, should be small with respect to the coherence length $\xi_c(T)$ in the direction perpendicular to the layers; then the layered structure is irrelevant. Hence, within this approach, a superconductor is considered as anisotropic but uniform. In particular, the quantized magnetic vortices are continuous lines oriented along the local magnetic induction $\mathbf{B}$. Dichalcogenides of transition metals, among which $NbSe_2$ is best studied, represent layered compounds for which the London approach is good due to relatively small T_c and consequently large ξ_c's.

However, many anisotropic materials (HTSC's are most prominent in this family) consist of the two-dimensional (2D) layers (Cu-O) where the superconductivity presumably resides. These are made into a 3D superconductor by a weak Josephson coupling between the layers. For most of these materials $\xi_c < s$ in a broad temperature range, and the anisotropic London theory should give way to the Lawrence-Doniach (LD) model.[6–8] The latter is not easy to implement due to its complicated formal structure (a set of nonlinear difference-differential equations for the order parameter and the magnetic field). In fact, up to now, only vortices parallel to the layers have been considered within the LD framework.[8–10] In this case, the normal core is absent as in well-studied Josephson vortices,[11] while at large distances from the vortex axis the LD description converges with that of London.

For an extreme anisotropy, as in Bi- and Tl-based compounds, a very weak interlayer Josephson coupling had prompted studies in which vortex lines are represented by stacks of 2D vortices residing in superconducting layers (so-called 2D pancakes) interacting exclusively via the magnetic field created in the interlayer space.[12–14] In other words, within this approach, the Josephson coupling and the interlayer currents are disregarded altogether. However, without these currents, tilted vortices cannot be formed in a tilted external field. In this model, the field component parallel to the layers penetrates the superconductor unperturbed, while the perpendicular component is responsible for the perpendicular vortices.

Clearly, both models (the 3D London and the 2D pancakes) are deficient as far as the description of real Josephson-coupled systems of 2D layers is concerned. The London model allows the currents to grow without limit when approaching the vortex core, whereas the actual Josephson currents are bound by a critical value which is further suppressed in the core. On the other hand, except for vortices along the c axis, the pancake model fails at large distances from the core, since Josephson currents are neglected in the domain where they are, in fact, comparable in value to the in-plane persistent currents. The failure of the pancake model to describe tilted vortices is a serious shortcoming to deal with in a better theory.

The idea of vortex kinks emerged in order to correct

 ©1992 The American Physical Society

deficiencies of the London theory. As applied to the vortex dynamics and fluctuation phenomena, the kinks were considered by Doniach *et al.*[15,16] In our work, however, we deal with equilibrium properties for which thermal fluctuations are irrelevant. Feinberg and Villard[17] suggested that, instead of being straight (along the direction of the magnetic induction **B**), the vortices are slightly wavy to take advantage of the lowest energy orientation along the layers. The model predicts that vortices will be *locked in* the orientation parallel to the layers for external fields close to the *ab* plane. Although pertinent, the prediction is not reliable quantitatively. As formulated, the model is able to treat only vortices with the radius of curvature exceeding the penetration depths, thus putting sharp kinks out of reach.

A more quantitative approach has been employed by Ivlev, Ovchinnikov, and Pokrovskii,[18] who assumed the vortices to form a staircase with a piece of the London vortex along *c* and another piece of a parallel London vortex in the *ab* plane. The authors obtained the London energy of a lattice of kinked vortices, which contains—in addition to a part corresponding to straight vortex lines—an extra contribution attributed to kinks. Being justifiable qualitatively, the kinked lattice is, in fact, implanted into the London theory. The results, if correct, should follow from minimization of the free-energy functional which models properly the highly anisotropic layered compounds. The LD model for layered Josephson-coupled superconductors provides such a free energy.

For layered materials, the most interesting angular region is situated near the *ab* plane. In this domain, deviations from the London model are the strongest. On the other hand, with the existing experimental accuracy of, for example, the intrinsic torque measurements,[19,20] this angular region can well be probed. The data available[20,21] show deviations in the measured torque from the 3D London prediction.[22]

In the following we develop an approach within the LD model, which yields equations similar to the sine-Gordon formalism of Josephson junctions. Solving the linear analog of these equations we obtain the line energy and the free energy of the flux-line lattice (FLL) for any orientation of vortices. We then compare different FLL structures. We argue that in compounds with extremely large anisotropy (as Tl-based HTSC) or in strong fields, a combined lattice made of coexisting sets of perpendicular and parallel vortices should occur for applied fields close to the *ab* plane. The idea about an independent response of layered superconductors to the parallel and perpendicular field components has been proposed by Kes *et al.* and later by Theodorakis[23,24] but the physical conditions for such a behavior have not been clearly formulated.

II. BASIC EQUATIONS

The LD free-energy functional has the form[6]

$$\mathcal{F}\{\Psi_n(\mathbf{r}),\mathbf{A}(\mathbf{R})\}=\frac{H_c^2 s}{4\pi}\sum_n\int d\mathbf{r}\left[\xi_{ab}^2\left|\left(-i\nabla+\frac{2\pi}{\phi_0}\mathbf{A}_n\right)\Psi_n\right|^2-|\Psi_n|^2+\tfrac{1}{2}|\Psi_n|^4\right.$$
$$\left.+\tfrac{1}{2}\rho(|\Psi_n|^2+|\Psi_{n+1}|^2-\Psi_n\Psi_{n+1}^*e^{-i\chi_{n,n+1}}-\Psi_n^*\Psi_{n+1}e^{i\chi_{n,n+1}})\right]+\int d\mathbf{R}\frac{h^2}{8\pi}. \tag{2.1}$$

Here $\mathbf{A}_n=(A_{nx},A_{ny})=[A_x(\mathbf{r},z=ns),A_y(\mathbf{r},z=ns)]$, $\mathbf{h}=\mathrm{curl}\mathbf{A}$, and

$$\chi_{n,n+1}=\frac{2\pi}{\phi_0}\int_{ns}^{(n+1)s}dz\,A_z\,.$$

Further, $\Psi_n(\mathbf{r})=|\Psi_n(\mathbf{r})|\exp[i\Phi_n(\mathbf{r})]$ is the order parameter in the layer n ($z=ns$), $\mathbf{r}=(x,y)$, $\mathbf{R}=(\mathbf{r},z)$, $\nabla=\partial/\partial\mathbf{r}$, the z axis is perpendicular to the layers, H_c is the bulk thermodynamic critical field, ξ_{ab} is the coherence length in the *ab* plane, and $\phi_0=\pi\hbar c/|e|$. Superconducting layers are assumed to have a negligible thickness.

One can derive the usual 3D Ginzburg-Landau free energy by replacing finite differences in Eq. (2.1) with derivatives $\partial/\partial z$.[6] The coherence lengths and the penetration depths so obtained are given by

$$\xi_c^2=s^2\rho/2,\quad \lambda_{ab}^2=\phi_0^2/8\pi^2H_c^2\xi_{ab}^2 \tag{2.2}$$

and by $\lambda_c/\lambda_{ab}=\xi_{ab}/\xi_c=\gamma$, where γ is the anisotropy ratio.

In the free energy (2.1), the dimensionless parameter $\rho\ll1$ characterizes the Josephson coupling between the layers; higher order terms in ρ are omitted (interaction with the next neighboring layers is proportional to ρ^2). The condition $\rho\ll1$ assures that the energy of the interlayer coupling $\rho sH_c^2/4\pi$ is small relative to the condensation energy $sH_c^2/8\pi$ (per unit area). Under this condition we have $\xi_c\ll s$, the length of inhomogeneity of the order parameter Ψ in the *c* direction.[7,8] In other words, the interlayer supercurrents are limited and weak, so that they cannot suppress the value of $|\Psi|$ in the layers.

In the following, we consider vortices oriented arbitrarily within the crystal. When they are parallel to the layers, the normal cores are absent.[8–10] For any other orientation, a disclike normal core is created in each layer crossed by the vortex. The condition $\rho\ll1$ has then an additional implication. It can be written, with the help of Eq. (2.2), as $\rho=2\xi_{ab}^2/s^2\gamma^2=2\xi_{ab}^2/\lambda_J^2\ll1$, where $\lambda_J=\gamma s$ is the Josephson length.[15] Regions near the vortex center in each layer, where the Josephson nature of the interlayer currents is important, have the size λ_J. The core size ξ_{ab} is much smaller than all other lengths of the problem: λ_J,λ_{ab}, or λ_c. Hence, $\rho=2\xi_{ab}^2/\lambda_J^2\ll1$ means that normal cores with suppressed order parameter constitute only a small fraction of the total volume, i.e., one can set $|\Psi|^2=1$. Thus, only the phases vary in $\Psi=|\Psi|e^{i\Phi}$, and we have, instead of Eq. (2.1), the free-energy functional with respect to the phases

$$\mathcal{F}\{\Phi_n(\mathbf{r}), \mathbf{A}(\mathbf{R})\} = \frac{\phi_0^2 s}{32\pi^3\lambda_{ab}^2}\sum_n \int d\mathbf{r}\left[\left(\nabla\Phi_n + \frac{2\pi}{\phi_0}\mathbf{A}_n\right)^2 + \frac{2}{\lambda_J^2}[1-\cos(\Phi_n - \Phi_{n+1} - \chi_{n,n+1})]\right] + \int d\mathbf{R}\frac{h^2}{8\pi}. \quad (2.3)$$

It is worth noting that as written the functional (2.1) is valid only near T_c. The validity domain of the functional (2.3) is broader. Actually, the energy of inhomogeneity given by the first term in square brackets is correct if the inhomogeneity scale exceeds $\xi_{ab}(T=0)$. This condition is always satisfied out of normal cores for applied fields H_{az} far from the perpendicular upper critical field. As written, the Josephson term in Eq. (2.3) is valid at any T. Thus, functional (2.3) can be used at all temperatures, the situation similar to the London equations which are applicable beyond the Ginzburg-Landau region.

Minimization of $\mathcal{F}$ with respect to $\mathbf{A}(\mathbf{R})$ and $\Phi_n(\mathbf{r})$ yields the system of equations for phases and fields in equilibrium. Varying $\mathbf{A}$ we obtain

$$(\text{curl curl}\mathbf{A})_\alpha = \frac{4\pi}{c}j_\alpha = -\frac{\phi_0 s}{2\pi\lambda_{ab}^2}\sum_n\left(\nabla\Phi_n + \frac{2\pi}{\phi_0}\mathbf{A}_n\right)_\alpha \delta(z-ns), \quad (2.4)$$

$$(\text{curl curl}\mathbf{A})_z = \frac{4\pi}{c}j_z = \frac{\phi_0}{2\pi\lambda_c^2 s}\sum_n \sin(\varphi_{n,n+1}) f_{n,n+1}(z), \quad (2.5)$$

where $\alpha = x, y$ and the *gauge invariant* phase difference $\Phi_n - \Phi_{n+1} - \chi_{n,n+1}$ is denoted as $\varphi_{n,n+1}$. The factor $f_{n,n+1}$ vanishes everywhere except for $ns < z < (n+1)s$, where it is unity. Minimization of $\mathcal{F}$ with respect to Φ_n yields

$$\nabla^2\Phi_n + \frac{2\pi}{\phi_0}\nabla\cdot\mathbf{A}_n = \frac{1}{\lambda_J^2}(\sin\varphi_{n,n+1} - \sin\varphi_{n-1,n}). \quad (2.6)$$

Here ∇^2 and $\nabla\cdot\mathbf{A}_n$ are the 2D Laplacian and 2D divergence in the xy plane.

Equations (2.4)–(2.6) form a complete system for the vector potential and the phases Φ_n, both of which are gauge dependent. Now we obtain an equation for phase differences $\varphi_{n,n+1}$, which is decoupled from equations for phases and fields. The gauge $A_z = 0$ provides a shortcut to obtain such an equation. As an immediate consequence of $A_z = 0$ we have $\chi_{n,n+1} = 0$. After integration of Eq. (2.5) over z from ns to $(n+1)s$, we obtain

$$\nabla\cdot(\mathbf{A}_{n+1} - \mathbf{A}_n) = \frac{\phi_0}{2\pi\lambda_c^2}\sin\varphi_{n,n+1}. \quad (2.7)$$

The left-hand side (lhs) here is expressed in terms of phase differences $\varphi_{n,n+1}$ with the help of Eq. (2.6) with the result

$$\lambda_J^2\nabla^2\varphi_{n,n+1} - (\lambda_J^2/\lambda_c^2)\sin\varphi_{n,n+1} - 2\sin\varphi_{n,n+1} + \sin\varphi_{n+1,n+2} + \sin\varphi_{n-1,n} = 0. \quad (2.8)$$

For vortices parallel to the layers, this equation has already been considered in Ref. 10; also, it was proposed in Ref. 25. The very fact that the phase differences $\varphi_{n,n+1}$ satisfy a *single* (be it finite-difference differential sine-Gordon) equation, which does not contain the field, is a remarkable simplification that makes further progress in determination of phases and fields possible. One, of course, can obtain this equation using a general gauge.

Boundary conditions for Eq. (2.8) are determined by positions of topological singularities (vortices). The singularities in phases $\Phi_n(\mathbf{r})$ at each position $\mathbf{r}_{n,\nu}$ are introduced as usual by $\text{curl}_z\nabla\Phi_n = 2\pi\delta(\mathbf{r} - \mathbf{r}_{n,\nu})$, which reads

$$\nabla_x\nabla_y\Phi_n - \nabla_y\nabla_x\Phi_n = 2\pi\sum_\nu \delta(\mathbf{r} - \mathbf{r}_{n,\nu}). \quad (2.9)$$

Writing this for n and $n+1$ and subtracting we obtain the boundary condition for $\varphi_{n,n+1}$:

$$\nabla_x\nabla_y\varphi_{n,n+1} - \nabla_y\nabla_x\varphi_{n,n+1} = 2\pi\sum_\nu[\delta(\mathbf{r} - \mathbf{r}_{n,\nu}) - \delta(\mathbf{r} - \mathbf{r}_{n+1,\nu})]. \quad (2.10)$$

Note that for vortices perpendicular to the layers ($\mathbf{r}_{n,\nu} = \mathbf{r}_{n+1,\nu}$) the singularities in $\varphi_{n,n+1}$ are absent.

For a vortex lattice, the boundary conditions imposed on $\varphi_{n,n+1}$ lead to certain relations between the magnetic induction $\mathbf{B}$ and averaged gradients of $\varphi_{n,n+1}$. The in-plane currents

$$\mathbf{j}_n = -\frac{c\phi_0}{8\pi^2\lambda_{ab}^2}\left(\nabla\Phi_n + \frac{2\pi}{\phi_0}\mathbf{A}_n\right) \quad (2.11)$$

and the field $\mathbf{h}$ are periodic in space. Writing Eq. (2.11) for n and $n+1$, subtracting, and taking into account that the average value of $\mathbf{j}$ over the unit cell is zero we obtain

$$\left\langle\frac{\partial}{\partial x}(\Phi_n - \Phi_{n+1})\right\rangle = \frac{2\pi}{\phi_0}\int_{ns}^{(n+1)s} dz\left\langle\frac{\partial A_x}{\partial z}\right\rangle$$

and a similar relation for $\langle\partial/\partial y(\Phi_n - \Phi_{n+1})\rangle$. Making use of $h_y = \partial A_x/\partial z$, we have

$$B_y = \langle h_y\rangle = (\phi_0/2\pi s)\langle\nabla_x\varphi_{n,n+1}\rangle, \qquad B_x = \langle h_x\rangle = -(\phi_0/2\pi s)\langle\nabla_y\varphi_{n,n+1}\rangle. \quad (2.12)$$

For vortices parallel to the layers, Eqs. (2.12) constitute boundary conditions for $\varphi_{n,n+1}$ because the singularities in x, y dependence of $\varphi_{n,n+1}$ are absent for this orientation.[10] It is worth noting that Eq. (2.8) and boundary conditions (2.12) are similar to those of the classic problem of a single Josephson junction, the difference being that in the multilayered system we should solve a *finite-difference sine-Gordon equation* instead of the usual sine-Gordon equation of a single junction; see, e.g., Ref. 11.

The general scheme of our approach is as follows. We first solve Eq. (2.8) for phase *differences*. Then we solve *linear* equations (2.4) and (2.6) where the rhs of Eq. (2.6) depends only on the already known $\varphi_{n,n+1}$ (the linear relation between $\nabla\Phi_n$ and $\mathbf{A}_n$ is established in Appendix B). Given the phase gradients and the vector potential, we can calculate the *equilibrium* value of the free energy F.

We conclude this part obtaining a more convenient form for the *equilibrium* free energy F. Here we can further benefit from the gauge $A_z = 0$. To this end we transform the magnetic part of (2.3):

$$\frac{c}{4\pi}\int h^2 d\mathbf{R} = s\sum_n \int (\mathbf{A}\cdot\mathbf{j}_n)\delta(z-ns)d\mathbf{r}\,dz = s\sum_n \int (\mathbf{A}_n\cdot\mathbf{j}_n)d\mathbf{r}. \tag{2.13}$$

This yields the free energy per unit volume in the form

$$F = s\sum_n \int d\mathbf{r}\left(-\frac{\phi_0}{4\pi c}\mathbf{j}_n\cdot\nabla\Phi_n + \frac{\phi_0^2}{16\pi^3 s^2\lambda_c^2}(1-\cos\varphi_{n,n+1})\right). \tag{2.14}$$

III. SINGLE TILTED VORTEX

Let a straight vortex lie in the x,z plane, contain the origin, and form angle θ with the c axis of the crystal; by this we imply that a discrete sequence of phase singularities situated in the layers form a straight line. In the layer n, the vortex center is at $x = (n-1/2)a$, $y = 0$, where $a = s\tan\theta$ (see Fig. 1). The condition (2.10) then assumes the form

$$(\nabla_x\nabla_y - \nabla_y\nabla_x)\varphi_{n,n+1} = 2\pi[\,\delta(x-na+a/2) - \delta(x-na-a/2)]\delta(y)\,. \tag{3.1}$$

Equations (2.8) and (3.1) suffice for determination of phase differences $\varphi_{n,n+1}$. According to (3.1), function $\varphi_{n,n+1}(\mathbf{r})$ depends on x and n via the combination $(x-na)$. Therefore, given $\varphi_{0,1}(x,y)$, one finds $\varphi_{n,n+1}$ by simple displacement: $\varphi_{n,n+1}(x,y) = \varphi_{0,1}(x-na,y)$.

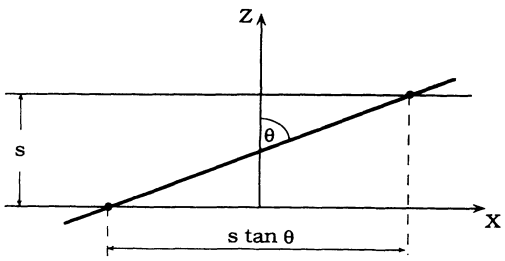

FIG. 1. The vortex axis (tilted line) is shown with respect to the layers (horizontal lines).

Hereafter we denote $\varphi_{0,1}(\mathbf{r})$ as $\varphi(\mathbf{r})$; its 2D Fourier transform (FT) is defined as

$$\varphi_{\mathbf{k}} = \int d\mathbf{r}\exp(-i\mathbf{k}\mathbf{r})\varphi(\mathbf{r}). \tag{3.2}$$

Let us further introduce the FT of $\nabla\varphi(\mathbf{r})$, i.e., $(\nabla\varphi)_{\mathbf{k}}$. Performing the FT of Eq. (2.8) one can write $(\nabla^2\varphi)_{\mathbf{k}} = ik_x(\nabla_x\varphi)_{\mathbf{k}} + ik_y(\nabla_y\varphi)_{\mathbf{k}}$. The FT of Eq. (3.1) reads

$$k_x(\nabla_y\varphi)_{\mathbf{k}} - k_y(\nabla_x\varphi)_{\mathbf{k}} = 4\pi\sin\frac{k_x a}{2}. \tag{3.3}$$

Due to the condition (3.1), the function $\varphi_{n,n+1}$ is singular and multivalued, so that there is a line (or lines) in the xy plane where the function experiences a jump of 2π. We choose it to be a straight line connecting the points $\mathbf{r}_n$ and $\mathbf{r}_{n+1}$. Then

$$(\nabla_x\varphi)_{\mathbf{k}} = ik_x\varphi_{\mathbf{k}}, \qquad (\nabla_y\varphi)_{\mathbf{k}} = ik_y\varphi_{\mathbf{k}} + \frac{4\pi}{k_x}\sin\frac{k_x a}{2}. \tag{3.4}$$

Note that $(\nabla\varphi)_{\mathbf{k}}$ is regular as $\mathbf{k}\to 0$. Substituting $(\nabla_x\varphi)_{\mathbf{k}}$ and $(\nabla_y\varphi)_{\mathbf{k}}$ in the FT of Eq. (2.8) we have for $\varphi_{\mathbf{k}}$

$$k^2\varphi_{\mathbf{k}} + \left(\frac{Q^2}{\gamma^2} + \frac{1}{\lambda_c^2}\right)W_{\mathbf{k}} = 4\pi i\frac{k_y}{k_x}\sin\frac{k_x a}{2}, \tag{3.5}$$

where

$$Q^2 = \frac{2}{s^2}(1-\cos k_x a), \quad W_{\mathbf{k}} = [\sin\varphi(\mathbf{r})]_{\mathbf{k}}, \tag{3.6}$$

and $k^2 = k_x^2 + k_y^2$.

Now we can express the currents $\mathbf{j}_n$ and the phase gradients $\nabla\Phi_n$ in terms of $\varphi_{n,n+1}(\mathbf{r})$; see Appendix B. Then we substitute them in Eq. (2.14) to obtain the equilibrium free energy (per unit length):

$$\epsilon = \epsilon_{\mathrm{EM}} + \frac{\phi_0^2\cos\theta}{128\pi^5}\int d\mathbf{k}\frac{1+\lambda_{ab}^2Q^2}{s^2\lambda_c^4k^2}|W_{\mathbf{k}}|^2 + \frac{\phi_0^2\cos\theta}{16\pi^3\lambda_c^2 s^2}\int d\mathbf{r}[1-\cos\varphi(\mathbf{r})],$$
$$\epsilon_{\mathrm{EM}} = \frac{\phi_0^2\cos\theta}{32\pi^3}\int d\mathbf{k}\frac{k^2+Q^2}{k^2[1+\lambda_{ab}^2(k^2+Q^2)]}. \tag{3.7}$$

Here ϵ_{EM} is the free energy of the tilted vortex in the pure electromagnetic (2D pancake) model ($\lambda_c = \infty$),[14] whereas other terms describe the effect of Josephson currents.

In closing the section we note that our formal procedure is similar to the usual London approach, in which a linear equation for the magnetic field is complemented with a singular rhs (see, e.g., Ref. 26). Here we have a nonlinear equation (2.8) for phase differences; our procedure to solve it under boundary condition (3.1) is equivalent to introducing a singular rhs

$$\pi\delta'(y)[\mathrm{sgn}(x-na+a/2) - \mathrm{sgn}(x-na-a/2)]. \tag{3.8}$$

IV. LINEAR APPROXIMATION

The London approximation can be obtained from our equations in two steps. First, $\sin\varphi_{n,n+1}$ is approximated by $\varphi_{n,n+1}$, then finite differences are replaced by derivatives

$$\varphi_{n,n+1} \approx -s\nabla_z\varphi + \tfrac{1}{2}s^2\nabla_z^2\varphi. \tag{4.1}$$

As has been mentioned, the function φ depends on x and n via the combination $(x - na)$. Hence, the expansion (4.1) corresponds in the Fourier space to the expansion $\cos k_x a$ and $\sin(k_x a/2)$ up to the second order in $k_x a$.

We will use the first step to obtain an approximation for the LD problem. Replacing $\sin\varphi_{n,n+1}$ by $\varphi_{n,n+1}$ but keeping the finite-difference character of Eq. (2.8) preserves the main feature of the LD model, namely, the limit, $j_0 = c\phi_0/8\pi^2 s\lambda_c^2$, imposed upon j_z by the Josephson character of the interlayer currents.[27] Evaluating the energy in the linear approximation we will keep logarithmically large terms, e.g., $\ln(\lambda_J/\xi_{ab})$, but neglect the terms of the order unity along with higher order terms in the small parameter ξ_{ab}/λ_J. In the exact LD approach, the maximum interlayer current is j_0 instead of πj_0 of the linear approximation. This difference, however, cannot change the logarithmically large contributions to the energy, thus making the results obtained within the linear approximation being valid with the logarithmic accuracy.

In the linear approximation, $W_{\mathbf{k}}$ of Eq. (3.5) coincides with $\varphi_{\mathbf{k}}$ and we obtain

$$\varphi_{\mathbf{k}} = \frac{4\pi i(k_y/k_x)\sin(k_x a/2)}{k^2 + 2\lambda_J^{-2}(1-\cos k_x a) + \lambda_c^{-2}}. \tag{4.2}$$

The current j_z is proportional to φ; the restriction upon j_z is, however, lost after the expansion of $\varphi_{\mathbf{k}}$ in $k_x a$.

Substituting (4.2) into (3.7) (after the replacement of $\cos\varphi$ with $1-\varphi^2/2$) we obtain the vortex free energy per unit length

$$\epsilon = \frac{\phi_0^2\cos\theta}{32\pi^3}\int_{k^2\le\xi_{ab}^{-2}} d^2\mathbf{k}\, f(k_x,k_y), \tag{4.3}$$

$$f(k_x,k_y) = \frac{k_x^2[1+\lambda_c^2(k^2+Q^2)] + Q^2[1+\lambda_{ab}^2(k^2+Q^2)]}{k_x^2(1+\lambda_{ab}^2Q^2+\lambda_c^2k^2)[1+\lambda_{ab}^2(k^2+Q^2)]}.$$

The 3D London expression for the free energy[2] is obtained from this equation expanding Q^2 in $k_x a$.

According to Eq. (4.2), there are three relevant length scales, a, λ_J, and λ_c in the coordinate dependence of the phase difference and hence of the interlayer currents. The fourth length is ξ_{ab} which determines the size of the normal core. Note that $a = s\tan\theta$ can take any place in the hierarchy $\xi_{ab} \ll \lambda_J \ll \lambda_c$, depending on the angle.

For all angles θ at the vortex periphery the currents are weak and the 3D anisotropic London approach is valid. In the vicinity of the core, the limitation imposed on the interlayer currents becomes important. We will see that the main contribution to the free energy of a single vortex still comes from the 3D London region, but the corrections to the London energy are strongly angular dependent.

To separate domains of the ab plain with different behavior we write Eq. (4.2) in the real space. Integrating over k_y and denoting $u = k_x a/2$, we have

$$\varphi(\mathbf{r}) = -2\,\mathrm{sgn}\,y\int_0^\infty \frac{du}{u}\sin u\cos\frac{2xu}{a}\exp\left(-\frac{|y|}{\lambda_J}Y(u)\right), \tag{4.4}$$

$$Y(u) = 2\sqrt{\frac{\lambda_J^2u^2}{a^2}+\sin^2u+\frac{s^2}{4\lambda_{ab}^2}}.$$

We see that the scale for the x dependence of φ is a, while the scale for y depends on the ratio $\lambda_J/a = \gamma/\tan\theta$. As we mentioned above, the London approach corresponds to $k_x a/2 = u \ll 1$.

A. Angular interval $\tan\theta < \xi_{ab}/s$

In this interval, $a \ll \xi_{ab}$, the main contribution to the integral (4.4) comes from $u \lesssim a/x$ [due to the oscillatory $\cos(2xu/a)$] or from $u \lesssim a/y$ (due to the exponential factor). At least one of the two quantities, a/x or a/y, is small since the point (x,y) must be out of the normal core and $a < \xi_{ab}$. Thus, one can set $\sin u \approx u$, and we conclude that *in this case the 3D London theory is valid everywhere out of the normal cores.*

B. Interval $\xi_{ab}/s \ll \tan\theta \ll \gamma$

Here $\xi_{ab} \ll a \ll \lambda_J$, and we obtain again the London result provided either x or y exceeds a. For shorter distances the main contribution comes from the domain $u \lesssim 1$ due to the factor $\sin u/u$. Then, $Y/\lambda_J \approx 2u/a$, i.e., both λ_J and λ_c drop off from Eqs. (4.2) and (4.4). This is a characteristic feature of the model with purely electromagnetic interaction between 2D pancakes. In fact, in this situation one can integrate in Eq. (4.4) to obtain the difference of two azimuthal angles:

$$\varphi(\mathbf{r}) = \tan^{-1}\frac{x-a/2}{y} - \tan^{-1}\frac{x+a/2}{y}. \tag{4.5}$$

For this reason we use for the domain $\xi_{ab} < r \ll a$ the term 2D core. Qualitatively, the size of the 2D core can be estimated within the London theory by determining the curve in the xy plane, where the London j_z reaches the critical Josephson value j_0; see Appendix A. The physical relevance of the 2D core is stressed by Feinberg.[28]

Notice that in this region φ is not small, and therefore the linear approximation breaks down. On the other hand, the in-plane currents here are much larger than the Josephson currents (which are *limited*), making the contribution of the latter altogether insignificant. The distribution of the intralayer currents within the 2D core is the same as that obtained within the electromagnetic model;[12–14] this distribution coincides with that of the *2D London* approach. Both 2D and 3D London regions are shown in Fig. 2.

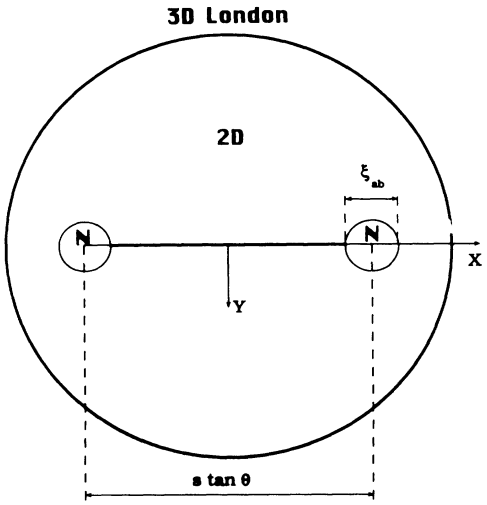

FIG. 2. Regions of different qualitative behavior of the phase difference (or of the interlayer currents) for the angular domain $\xi_{ab}/s \ll \tan\theta \ll \gamma$. The normal cores ($N$), 2D and the 3D London regions are shown schematically. The size of the 2D region is of the order $s\tan\theta$. The positions of normal cores correspond to the two pancake centers in the adjacent layers.

C. Interval $\gamma \ll \tan\theta \ll \lambda_c/s$

In this most interesting interval of angles, $a \gg \lambda_J$, and for $x \gg a$ or $y \gg \lambda_J$, the main contribution to the integral (4.4) comes from $u \ll 1$. One then has $\sin u \approx u$, in other words, $x \approx a$ and $y \approx \lambda_J$ give the internal boundary of the 3D London domain shown schematically in Fig. 3; this estimate can also be obtained from the London j_z, see Appendix A. Inside this boundary, within circles $r \ll \lambda_J$ centered at two singularities, we again have the 2D regions where the phases $\Phi_n(\mathbf{r})$ are given by the corresponding azimuthal angle.

There is yet another region of a different behavior between the 2D circles which we call the Josephson string, see Fig. 3. We notice that according to (4.4), φ has a discontinuous jump of 2π when one crosses the line connecting the centers of two 2D vortices.[29] It is this jump which causes the anomalous behavior of the Fourier transform in (3.4), $(\nabla_y\varphi)_{\mathbf{k}} \neq ik_y\varphi_{\mathbf{k}}$. The jump is introduced by the boundary condition (3.1).

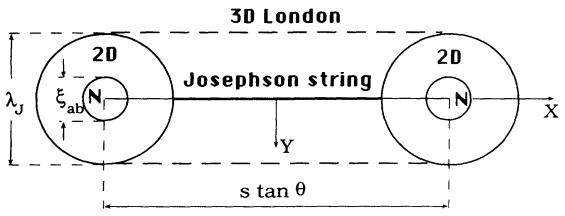

FIG. 3. Normal cores, 2D cores, the Josephson string, and the 3D London region are shown schematically for a tilted vortex in the angular domain $\gamma \ll \tan\theta \ll \lambda_c/s$.

V. EVALUATION OF INTEGRALS

In this section we calculate the line energy (4.3) with the logarithmic accuracy; the reader may be referred directly to the next section for the results of this derivation. To calculate the integral in (4.3), which is logarithmically divergent at $\xi_{ab} \to 0$, we replace the region of integration $k \leq \xi_{ab}^{-1}$ by the infinite strip parallel to the k_x axis of the width $2\xi_{ab}^{-1}$:

$$\int_{k^2\leq\xi_{ab}^{-2}} d^2\mathbf{k}\, f(\mathbf{k}) = 4\int_0^{+\infty} dk_x \int_0^{\xi_{ab}^{-1}} dk_y\, f(\mathbf{k}) . \tag{5.1}$$

Such a replacement is possible because in the direction k_x the function $f(k_x, k_y)$ decreases faster than in k_y as k increases. In fact, after the expansion of Q^2 in $k_x a$ in the denominator of Eq. (4.3) we have

$$1 + \lambda_{ab}^2 Q^2 + \lambda_c^2 k^2 \approx 1 + (\lambda_{ab}^2\tan^2\theta + \lambda_c^2)k_x^2 + \lambda_c^2 k_y^2 ,$$
$$1 + \lambda_{ab}^2(Q^2 + k^2) \approx 1 + \lambda_{ab}^2(k_x^2\sec^2\theta + k_y^2) . \tag{5.2}$$

Note that integration over a strip oriented along k_y yields a different result due to the anisotropy of $f(k_x, k_y)$, see Appendix C.

Next, we substitute k_x with $(u + 2\pi m)/a$, where m is an integer. Then, integration over k_x is replaced by the integral over u in the interval $[0, 2\pi]$ and the sum over m,

$$\epsilon = \frac{\phi_0^2\cos\theta}{32\pi^3 a}\sum_{m=-\infty}^{\infty}\int_0^{2\pi} du \int_0^{\xi_{ab}^{-1}} dk_y\, f\left(\frac{u+2\pi m}{a}, k_y\right) . \tag{5.3}$$

The sum is evaluated with the help of Eq. (B6). We obtain as a result

$$\epsilon = \frac{s\phi_0^2\sin\theta}{16\pi^3}\int_0^{\xi_{ab}^{-1}} dk_y \int_0^{\pi} du\left[\frac{2s^{-2}}{1+\lambda_{ab}^2Q^2+\lambda_c^2k_y^2} + \left(\frac{1}{1+\lambda_{ab}^2Q^2} - \frac{1}{1+\lambda_{ab}^2Q^2+\lambda_c^2k_y^2}\right)\frac{Q^2\sinh X_c}{X_c(\cosh X_c - \cos u)}\right.$$
$$\left. + \frac{\sinh X_a}{\lambda_{ab}^2(1+\lambda_{ab}^2Q^2)X_a(\cosh X_a - \cos u)}\right] , \tag{5.4}$$

where $Q^2 = 2s^{-2}(1-\cos u)$ and

$$X_c = a\lambda_c^{-1}(1+\lambda_{ab}^2 Q^2 + \lambda_c^2 k_y^2)^{1/2},$$

$$X_a = a\lambda_{ab}^{-1}[1+\lambda_{ab}^2(Q^2+k_y^2)^{1/2}].$$

The first term in square brackets yields

$$\epsilon_1 \approx \frac{\phi_0^2 \sin\theta}{16\pi^2\lambda_{ab}\lambda_c}\ln\frac{\lambda_{ab}}{s}. \tag{5.5}$$

Terms of the order unity are neglected with respect to the large $\ln(\lambda_{ab}/s)$.

To evaluate the remaining integrals we divide the integration interval over k_y in two. In the first $k_y < a^{-1}$, both $X_c \le 1$ and $X_a \le 1$, and the integrand can be expanded in X_c and X_a. In the rest of the integration domain, $a^{-1} < k_y < \xi_{ab}^{-1}$, both X_c and X_a are large and one can set $\sinh X_{a,c}/(\cosh X_{a,c} - \cos u) \approx 1$.

For $\tan\theta > \xi_{ab}/s$ the result from the region $0 \le k_y \le a^{-1}$ is

$$\epsilon_2 \approx \frac{\phi_0^2 \sin\theta}{16\pi^2\lambda_{ab}\lambda_c}\left([(1+\eta^2)^{1/2}-1]\ln\frac{\lambda_c}{a} + \tfrac{1}{2}\ln(1+\eta^2) + \eta\ln[(1+\eta^2)^{1/2}-\eta]\right), \tag{5.6}$$

where

$$\eta = \gamma\cot\theta. \tag{5.7}$$

The contribution of the region $k_y > a^{-1}$ is

$$\epsilon_3 \approx \frac{\phi_0^2\cos\theta}{16\pi^2\lambda_{ab}^2}\ln\frac{\lambda_J[(1+\eta^2)^{1/2}-\eta]}{\xi_{ab}}. \tag{5.8}$$

VI. ENERGY OF TILTED VORTICES

A. Line energy

Collecting all contributions to ϵ for $\tan\theta > \xi_{ab}/s$, Eqs. (5.5), (5.6), and (5.8), we obtain the line energy

$$\epsilon(\theta) = \frac{\phi_0^2}{16\pi^2\lambda_{ab}\lambda_c}\left((1+\eta^2)^{1/2}\ln\frac{\lambda_c C_1\eta}{\lambda_J} + \eta\ln\frac{\lambda_J C_2[(1+\eta^2)^{1/2}-\eta]^2}{\xi_{ab}} - \ln\frac{C_3\eta}{(1+\eta^2)^{1/2}}\right). \tag{6.1}$$

The constants C_1, C_2, and C_3 of the order unity represent corrections to the logarithmic terms. They are included because their contribution may not be small in comparison with bare logarithms; we will see that the constants are relevant for determination of the vortex lattice structure. Within the linear approximation we have found numerically that $\ln(C_1/C_3) = 2.06$ and $\ln C_2 = -0.9$ in the limit $\eta \ll 1$.

We note that the first term in (6.1) comes from the 3D London region, and the logarithm's argument is the ratio of the upper and the lower boundaries of this region in the ab plane. The second term is due to the 2D core limited by the circles with radii ξ_{ab} and λ_J. As we have mentioned, the character of large logarithmic terms should be the same in the exact LD. Thus, the expression (6.1), obtained in linear approximation, provides the LD free energy with logarithmic accuracy. In other words, in the exact LD free energy, only the values C_1, C_2, and C_3 differ from those obtained in the linear approximation. To calculate the constants, we have to solve Eq. (3.5) beyond the linear approximation. In principle, this can be done numerically. In fact, $\epsilon(\pi/2)$ has already been evaluated;[9] it gives $\ln(C_1/C_3) = 1.12$.

The total vortex energy should contain the contribution of the normal core:

$$\epsilon_{\rm core}(\theta) = \frac{H_c^2}{4\pi}\xi_{ab}^2\cos\theta\ln C_4 = \frac{\phi_0^2\cos\theta}{16\pi^2\lambda_{ab}^2}\ln C_4, \tag{6.2}$$

where $\ln C_4 \approx 0.5$.[30] For $\tan\theta \gg \gamma$ ($\eta \ll 1$), the second term in (6.1) has the same prelogarithm factor as in Eq. (6.2). Then, one can incorporate the core correction into the line energy by adjusting the constant C_2.

As is seen from (6.1), the contribution of the 2D core (the second term) vanishes for $\tan\theta \ll \xi_{ab}/s$. In the angular interval $\xi_{ab}/s \ll \tan\theta \ll \gamma$ we obtain

$$\epsilon = \frac{\phi_0^2\cos\theta}{16\pi^2\lambda_{ab}^2}\left(\ln\frac{\lambda_{ab}C_1C_2}{2\xi_{ab}\cos\theta} + \frac{\tan^2\theta}{2\gamma^2}\ln\frac{\lambda_{ab}C_1}{s\tan\theta}\right), \tag{6.3}$$

where the first term coincides with the corresponding London result.

It is instructive to compare the line energies within London, LD, and purely electromagnetic (EM) [$\gamma = \infty$ (Ref. 14)] models for high angles $\tan\theta \gg \gamma$:

$$\epsilon_L = \frac{\phi_0^2}{16\pi^2\lambda_{ab}^2}\left(\frac{1}{\gamma}+\frac{1}{2}\gamma\cos^2\theta\right)\ln\frac{\lambda_c}{\xi_{ab}}, \tag{6.4}$$

$$\epsilon_{\rm LD} = \frac{\phi_0^2}{16\pi^2\lambda_{ab}^2}\left(\frac{1}{\gamma}\ln\frac{\lambda_c}{\lambda_J} + \cos\theta\ln\frac{\lambda_J}{\xi_{ab}}\right), \tag{6.5}$$

$$\epsilon_{\rm EM} = \frac{\phi_0^2}{16\pi^2\lambda_{ab}^2}\cos\theta\ln\frac{\lambda_{ab}}{\xi_{ab}\cos\theta}, \tag{6.6}$$

where the factors C are omitted. The London model overestimates the line energy of parallel vortices, while underestimating the tilting energy ($\cos^2\theta$ instead of LD's $\cos\theta$). Within the EM model, the energy of parallel vortices is zero (the parallel field penetrates unperturbed); the tilting energy is overestimated due to the absence of the screening by interlayer currents.

As was mentioned above, the second term in (6.5) comes from the 2D core. We obtain now this term using qualitative arguments. The currents in the ab plane are given by Eq. (2.11), and the energy due to these currents is proportional to $\int j_\parallel^2 dx\,dy$. The value $\nabla\Phi_n$ decreases as $2\pi/r$ because $\oint \nabla\Phi_n\cdot d\mathbf{l} = 2\pi$ for a path round the point $r=0$. Then the spatial variation of $j_\parallel$ depends on the behavior of the vector potential $\mathbf{A}_n$.

In a perpendicular vortex, for $r < \lambda_{ab}$, $|\mathbf{A}|$ is small relative to $j_\parallel \propto \phi_0/\lambda_{ab}^2 r$; at larger r's, the current $j_\parallel$ is

exponentially small (the term $\nabla\Phi_n$ in $j_\parallel$ is compensated by $\mathbf{A}_n$). Thus the energy per pancake is proportional to $\phi_0^2 s\lambda_{ab}^{-2}\ln(\lambda_{ab}/\xi_{ab})$ as in the London case.

For a single pancake in a multilayer system, due to the screening of the magnetic field by all other superconducting layers, the vector potential is small everywhere; it cannot change the $1/r$ dependence of $j_\parallel$ at any distance. The cut-off or magnetic energy is determined by the system size or, in the presence of other pancakes in the case of tilted vortices, by the length $\lambda_{ab}a/s$ [Eq. (6.6)]. In the Josephson coupled systems, in the region $r > r_0$ where j_z does not exceed the critical value j_0 we have the 3D London behavior. Comparing $j_z \propto \phi_0/\lambda_{ab}^2\gamma r$ ($j_z \propto j_\parallel/\gamma$) (see Appendix A for details) with j_0 for $\tan\theta < \gamma$ we obtain the radius of the crossover region: $r_0 = \gamma s = \lambda_J$. The energy contribution of the 2D region $\xi_{ab} < r < \lambda_J$ is proportional to $\phi_{ab}^2 s\lambda_{ab}^{-2}\ln(\lambda_J/\xi_{ab})$ per pancake which gives (6.5) for the line energy.

B. Energy of the vortex lattice

For a vortex lattice we should solve Eq. (2.8) under boundary conditions (2.10), in which the core loci are periodically arranged.

Due to the periodicity of the vortex lattice, the Fourier components $\varphi_{\mathbf{k}}$ are nonzero only for $\mathbf{k}$ coinciding with vectors of the reciprocal lattice $\mathbf{g}$ in the ab plane. Therefore, to obtain the lattice free energy density, we replace the integral over $\mathbf{k}$ in Eq. (3.7) by the sum over $\mathbf{g}$ truncated at $|\mathbf{g}| \approx \xi_{ab}^{-1}$:

$$\frac{1}{(2\pi)^2}\int d\mathbf{k} \to \frac{B^2\cos\theta}{\phi_0^2}\sum_{\mathbf{g}}. \tag{6.7}$$

The integral over $\mathbf{r}$ in Eq. (3.7) is restricted to the lattice unit cell; the prefactor ϕ_0^2 is replaced with $\phi_0 B$.

For the sake of simplicity we consider hereafter rectangular lattices. In moderate fields, $H_{c1} \ll H \ll H_{c2}$, we can utilize the linear approximation, as long as the lattice size in the x direction, $l_B\gamma^{-1/2}/\cos\theta$ ($l_B^2 = \phi_0/B$),[5] exceeds a, the size of the Josephson string in which the approximation fails. This condition is fulfilled in applied yields

$$H_a \ll \frac{H_0}{\sin^2\theta}, \quad H_0 = \frac{\phi_0}{s^2\gamma}. \tag{6.8}$$

This condition also assures that the 2D cores do not overlap in the y direction. Thus, implementing the rule (6.7), we can use Eq. (4.3) for the line energy, obtained in the linear approximation. The reciprocal lattice vectors $\mathbf{g}$ in xy plane are

$$\begin{aligned} g_x &= g_{0x}p, \quad g_{0x} = 2\pi l_B^{-1}(\cos\theta)^{1/2}(1+\eta^{-2})^{-1/4}, \\ g_y &= g_{0x}q, \quad g_{0y} = 2\pi l_B^{-1}(\cos\theta)^{1/2}(1+\eta^{-2})^{1/4}, \end{aligned} \tag{6.9}$$

where p,q are integers. The term $p = q = 0$ in the sum over p, q yields $B^2/8\pi$. Evaluating the rest of the sum, we replace summation with integration, thus obtaining the same integral as in Eq. (5.1) but now with lower limits of integrations over k_x and k_y given by g_{0x} and g_{0y}, respectively.

We then obtain the free-energy density of a tilted lattice for $\tan\theta > \xi_{ab}/s$:

$$F(\mathbf{B},\eta) = \frac{B^2}{8\pi} + \frac{\phi_0 B\sin\theta}{16\pi^2\lambda_{ab}^2\gamma}\left((1+\eta^2)^{1/2}\ln\frac{l_B\eta^2\gamma^{-1/2}C_1'}{s(1+\eta^2)^{1/4}} + \eta\ln\frac{\lambda_J C_2'[(1+\eta^2)^{1/2}-\eta]^2}{\xi_{ab}} - \ln\frac{\eta C_3'}{(1+\eta^2)^{1/2}}\right), \tag{6.10}$$

if $\eta \gg s\gamma^{1/2}/l_B = (B/H_0)^{1/2}$. For $\eta \gg 1$, the main logarithmically large term coincides with that of the London model. Note that the angular domain for Eq. (6.10) is quite broad: $\tan\theta \ll \gamma(H_0/B)^{1/2}$. In the opposite limit, $\tan\theta \gg \gamma(H_0/B)^{1/2}$, we obtain

$$F(\mathbf{B},\eta) = \frac{B^2}{8\pi} + \frac{\phi_0 B\sin\theta}{16\pi^2\lambda_{ab}^2\gamma}\left(\ln\frac{l_B C_1}{s\gamma^{1/2}} + \eta\ln\frac{\lambda_J C_2}{\xi_{ab}}\right). \tag{6.11}$$

The energy (6.11) in the interval $\eta \ll s\gamma^{1/2}/l_B$ coincides with the results of the kink model,[18] in which the vortex is made of London segments of the length $s\tan\theta$ parallel to the layers, separated by short London kinks of the length s parallel to c. It is worth noting that the kink model reproduces correctly the 2D core contribution [proportional to η in (6.11)], the leading one as far as $\partial F/\partial\theta$ for $\theta \to \pi/2$ is concerned. In particular, this term is responsible for the lock-in transition and an anomalous torque at large angles, discussed in following sections. This term in the kink model comes from the short pieces of vortices along c. Thus, these pieces account properly for the contribution of the 2D cores where the currents are mainly in the ab plane, as it is for perpendicular London vortices.

VII. PHASE DIAGRAM

Due to the normal and 2D cores, the tilted vortex becomes energetically unfavorable at high angles, and the phase transition from the tilted to the parallel vortex lattice (the lock-in transition) may occur.[17,31,18,32] We will show that in fact this takes place if $\lambda_J < \lambda_{ab}$. The situation is more complicated if $\lambda_J > \lambda_{ab}$.

The applied field $\mathbf{H}_a$ at which the lock-in transition takes place, depends on the sample shape; it occurs at small H_{az} where the magnetization M_z is comparable with H_{az}. We consider the sample as a rotational ellipsoid with demagnetization factors $n_x = n_y$ and $n_z = 1 - 2n_x$. Usually available samples are thin platelets with the c axis perpendicular to the plate so that $n_x \ll 1$. The proper thermodynamic potential for a

given $\mathbf{H}_a$ is $\tilde{G}(\mathbf{H}_a) = F(\mathbf{B}) - B^2/8\pi + (\mathbf{B} - \mathbf{H}_a)\mathbf{M}/2$.[33] Magnetization $\mathbf{M}$ is related to the applied field via $H_{a,i} = B_i - 4\pi M_i(1 - n_i)$ with $i = x, z$; therefore

$$\tilde{G}(\mathbf{H}_a; \mathbf{B}) = F(\mathbf{B}) - \frac{B^2}{8\pi} + \frac{(B_x - H_{ax})^2}{8\pi(1 - n_x)} + \frac{(B_z - H_{az})^2}{8\pi(1 - n_z)}. \tag{7.1}$$

The conditions $\partial\tilde{G}/\partial B = \partial\tilde{G}/\partial\theta = 0$ determine the magnitude and the orientation of $\mathbf{B}$ in equilibrium at a given $\mathbf{H}_a$.

A. Boundary of the Meissner phase

For $B \to 0$, $F = \epsilon(\theta)B/\phi_0$. It is convenient in this situation to work in terms of the internal field $\mathbf{H} = 4\pi(\partial F/\partial\mathbf{B})$, with components $H_x = H_{ax}/(1 - n_x)$ and $H_z = H_{az}/(1 - n_z)$. While differentiating F with respect to $B_{x,z}$ we use $\theta = \tan^{-1}(B_x/B_z)$ to obtain

$$(\phi_0/4\pi)H_x = \epsilon'(\theta)\cos\theta + \epsilon(\theta)\sin(\theta), \tag{7.2}$$

$$(\phi_0/4\pi)H_z = -\epsilon'(\theta)\sin\theta + \epsilon(\theta)\cos(\theta). \tag{7.3}$$

The minimum value of $H = (H_x^2 + H_z^2)^{1/2}$ determines the Meissner boundary in the plane (H_x, H_z); the angle θ can be considered as a running parameter for the Meissner curve.[34,32] In general, for a given orientation α of $\mathbf{H}$, there are more than one points on the curve $H_z(H_x)$ [$H(\alpha)$ is multivalued]. Writing the variations dH_x and dH_z due to a small change $d\theta$, we obtain the slope of the Meissner boundary $H_z(H_x)$ being negative everywhere (except $\theta = 0$):

$$dH_z/dH_x = -\tan\theta. \tag{7.4}$$

Equations (7.2)–(7.4) are quite general. In our case the line energy $\epsilon(\theta)$ is given by Eq. (6.1) for $\tan\theta > \xi_{ab}/s$ and by the London result (A9) for smaller angles. Particular values we need for our analysis are $\epsilon(0) = \phi_0 H_{c1,\perp}/4\pi$ and $\epsilon(\pi/2) = \phi_0 H_{c1,\parallel}/4\pi$ with

$$H_{c1,\perp} = \frac{\phi_0}{4\pi\lambda_{ab}^2}\ln\frac{\lambda_{ab}}{\xi_{ab}}, \quad H_{c1,\parallel} = \frac{\phi_0}{4\pi\lambda_{ab}\lambda_c}\ln\frac{\lambda_{ab}}{s} \tag{7.5}$$

(the constants C are omitted for brevity). Also, $\epsilon'(0) = 0$ and $\epsilon'(\pi/2) = -\phi_0 H_J/4\pi$ with

$$H_J = \frac{\phi_0}{4\pi\lambda_{ab}^2}\ln\frac{\lambda_J}{\xi_{ab}}. \tag{7.6}$$

Let us consider two cases.

1. $H_{c1,\perp} > H_J$

Equations (7.2) and (7.3) yield two points, L_1 and L_2, at the boundary between the Meissner phase and the mixed phase of *tilted* vortices (ϵ for a tilted vortex is used):

$$L_1: \quad \theta = 0, \quad H_x = 0, \quad H_z = H_{c1,\perp}, \quad dH_z/dH_x = 0;$$

$$L_2: \quad \theta = \pi/2, \quad H_x = H_{c1,\parallel}, \quad H_z = H_J, \quad dH_z/dH_x = \infty.$$

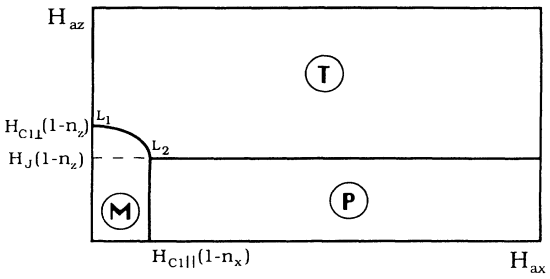

FIG. 4. Phase diagram in the plane (H_x, H_z) for $H_J < H_{c1,\perp}$. Domains of the Meissner state (M), of the tilted vortex lattice (T), and of the lattice locked in the parallel orientation (P) are shown schematically.

The phase boundary is shown in Fig. 4; the part of the curve between L_1 and L_2 can be evaluated numerically.

When one moves along the Meissner boundary from L_1 to L_2, θ increases. At point L_2, the vortices reach the parallel orientation, while the applied field is still at an angle α_c such that

$$\tan\alpha_c = \frac{1 - n_x}{1 - n_z}\frac{H_{c1,\parallel}}{H_J}. \tag{7.7}$$

For $\alpha > \alpha_c$, vortices stay parallel. To see that this is the case, one finds the Meissner boundary for parallel vortices using $F = \epsilon(\pi/2)B_x/\phi_0$: $H_x = H_{c1,\parallel}$ for any H_z. On the phase diagram, Fig. 4, this is a vertical line terminating at L_2. This line goes smoothly into the curve L_2L_1. When one crosses L_2, moving along the Meissner boundary, the parallel phase goes over to the tilted one in a continuous manner, which corresponds to the second-order phase transition. This type of the phase diagram has been considered in Ref. 32.

2. $H_{c1,\perp} < H_J$

In this case, point L_2 is situated above L_1 (see Fig. 5). Since the phase boundary (starting at L_1 with zero

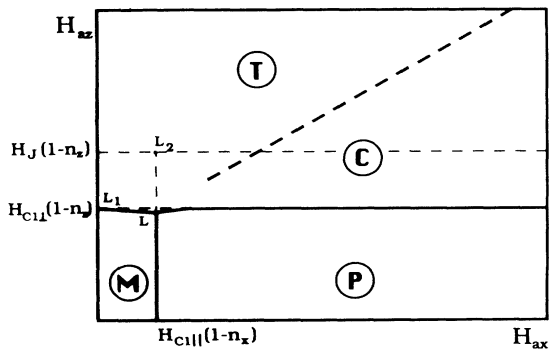

FIG. 5. Phase diagram in the plane (H_x, H_z) for $H_J > H_{c1,\perp}$. Domains of the Meissner phase (M), of the tilted vortex lattice (T), of the lattice locked in the parallel orientation (P), and of the combined lattice (C) are shown schematically. Tilted lattice does not exist below the line $H_{az} = H_J(1 - n_z)$ for $H_{ax} \gg H_{c1,\parallel}(1 - n_x)$.

slope) has a negative slope [see Eq. (7.4)], point L_2 is out of the phase boundary. The curve reaches the boundary of the parallel vortices at point L, which corresponds to the angle α slightly larger than $\tan^{-1}(H_{c1,\parallel}/H_{c1,\perp})$. One can show that when α moves from L_1 to L, the angle θ changes from 0 to about $1/\gamma \ll 1$. Therefore, when crossing point L along the boundary, the direction of nucleating vortices jumps from $\theta \sim 1/\gamma$ to $\pi/2$. This is a first-order phase transition.

B. Boundary of the tilted lattice

As the next step we determine the boundary for the *existence* of the tilted lattice in fields $H_0 \gg H_{ax} \gg \phi_0/\lambda_{ab}^2 \tan\theta$. Minimizing $\tilde{G}$ of Eq. (7.1) relative to $\mathbf{B}$ with $F(\mathbf{B})$ of Eq. (6.1), we obtain $B_x \approx H_{ax}$ and $B_z \approx H_{az} - H_J(1-n_z)$. Thus in large fields close to the ab orientation, the line $H_{az} \approx H_J(1-n_z)$ sets the boundary under which the tilted lattice cannot exist. For $H_J < H_{c1,\perp}$ this line starts from point L on the Meissner boundary. Then the phase diagram of Fig. 4 is possible where all boundaries are lines of the second-order phase transition. The potential $\tilde{G}_t(\mathbf{H}_a)$ for the tilted lattice in equilibrium near the boundary, for $B_z = H_{az} - H_J(1-n_z) \ll H_{ax}^{3/2}/H_0^{1/2}\gamma$, is obtained from Eq. (7.1):

$$\tilde{G}_t(\mathbf{H}_a) = \frac{H_{ax}\phi_0}{32\pi^2\lambda_{ab}^2\gamma}\ln\frac{H_0}{H_{ax}} + \frac{H_{az}H_J}{4\pi}, \tag{7.8}$$

where higher-order terms in $(1-n_z)$ and B_z/H_{ax} are omitted. In the interval $\eta = H_{az}\gamma/H_{ax} \gg 1$ the result is similar to the London one:

$$\tilde{G}_t(\mathbf{H}_a) = \frac{H_{az}\phi_0}{32\pi^2\lambda_{ab}^2}\ln\frac{H_{c2,\perp}C_1'C_2'}{H_{az}}. \tag{7.9}$$

Again, the factor $C_1'C_2'$ may be different from that of London due to the contribution of 2D cores.

For $H_J > H_{c1,\perp}$ in the interval $H_{c1,\perp}(1-n_z) < H_{az} < H_J(1-n_z)$ the tilted lattice is impossible. However, the parallel lattice does not correspond to equilibrium because creation of perpendicular vortices lowers the energy. We conclude that a new type of vortex arrangement should occur for $H_J > H_{c1,\perp}$ which consists of coexisting parallel and perpendicular vortices. We call this arrangement the combined lattice. The transition from the parallel to combined lattice is of the second order; as H_{az} increases, on the line $H_{az} = H_{c1,\perp}(1-n_z)$, the perpendicular vortex lattice develops starting from zero density. The boundary between combined and tilted lattices is the first-order transition line. To find this line one should know the free energy of the combined lattice.

C. Combined lattice

Let us show first that the interaction energy of parallel and perpendicular vortices is zero. For this purpose we use Eq. (2.14) and find the interaction term:

$$F_{\rm int} = -\frac{\phi_0}{4\pi c}\sum_n \int d\mathbf{r}\cdot\left(\mathbf{j}_n^{(\parallel)}\nabla\Phi_n^{(\perp)} + \mathbf{j}_n^{(\perp)}\nabla\Phi_n^{(\parallel)}\right). \tag{7.10}$$

The solution for parallel vortices (along x axis) is given by x independent $\varphi_{n,n+1}$, i.e., both $\nabla_x\Phi_n^{(\parallel)}$ and $j_{n,x}^{(\parallel)}$ vanish. In the Fourier representation $j_{n,y}^{(\parallel)}$ and $\nabla_y\Phi_n^{(\parallel)}$ are proportional to $\delta(k_x)$. For perpendicular vortices we have

$$(\nabla_y\Phi_n^{(\perp)})_{\mathbf{k}} = -\frac{2\pi i k_x}{k^2}\sum_\nu \exp(i\mathbf{k}\cdot\mathbf{r}_\nu),$$
$$(j_{n,y}^{(\perp)})_{\mathbf{k}} = -\frac{\phi_0 c}{16\pi^3}\frac{ik_x}{1+\lambda_{ab}^2k^2}\sum_\nu \exp(i\mathbf{k}\cdot\mathbf{r}_\nu). \tag{7.11}$$

All remaining terms in (7.10) vanish since $k_x\delta(k_x) = 0$.

Now, starting from the parallel lattice in the parallel field and turning on H_{az}, one can create new perpendicular vortices (the cost in energy is $\phi_0 H_{C1,\perp}/4\pi$ per one vortex). The alternative is to tilt the existing parallel lattice (at a cost of $\phi_0 H_J/4\pi$). For $H_J < H_{c1,\perp}$ the tilting is favorable, while for $H_J > H_{c1,\perp}$ formation of the combined lattice takes place.

Taking into account that within the combined lattice, perpendicular and parallel vortices form independent systems, we conclude that at given B_x and B_z the component B_z determines the density and the structure of the lattice of perpendicular vortices, while the B_x component is responsible for the parallel lattice. The free energy of the combined lattice for high $H_{ax} \gg H_{c1,\parallel}$ and $H_{az} \ll \phi_0/\lambda_{ab}^2$ (high density of parallel vortices and low density of perpendicular ones) is

$$F_c(\mathbf{B}) = \frac{B_x^2}{8\pi} + \frac{B_x\phi_0}{32\pi^2\lambda_{ab}^2\gamma}\ln\frac{H_0}{B_x} + \frac{B_z H_{c1,\perp}}{4\pi}. \tag{7.12}$$

To obtain the free energy for a dense perpendicular lattice we should replace the last term by $B_z^2/8\pi + (B_z\phi_0/32\pi^2\lambda_{ab}^2)\ln(H_{c2,\perp}/B_z)$.

Minimizing $\tilde{G}(\mathbf{B};\mathbf{H}_a)$ with respect to B_x gives $B_x \approx H_{ax}$. While minimizing relative to B_z, we should take into account that $1-n_z \ll 1$. Then we obtain for the combined lattice with a dilute perpendicular part:

$$\tilde{G}_c(\mathbf{H}_a) = \frac{H_{ax}\phi_0}{32\pi^2\lambda_{ab}^2\gamma}\ln\frac{H_0}{H_{ax}} + \frac{H_{az}H_{c1,\perp}}{4\pi} - \frac{H_{az}^2 + H_{c1,\perp}^2(1-n_z)}{8\pi}. \tag{7.13}$$

Comparing $\tilde{G}_t(\mathbf{H}_a)$ of Eq. (7.8) and $\tilde{G}_c(\mathbf{H}_a)$ just obtained, we see that for low H_{az} and $H_J > H_{c1,\perp}$ the combined lattice has lower energy. For smaller angles, $\tan\theta \ll \gamma$, the main logarithmic terms of $\tilde{G}_t(\mathbf{H}_a)$ and $\tilde{G}_c(\mathbf{H}_a)$ are the same. However, the linear approximation used so far is not sufficient to provide the higher-order terms. In the interval of angles $\tan\theta \ll \xi_{ab}/s$, the London model applies and therefore the tilted lattice has lower energy, see Appendix A. Thus the location of the first-order transition line can be limited only by inequalities $sH_{ax}/\xi_{ab} > H_{az} - H_J(1-n_z) > H_{ax}/\gamma$. The phase diagram for the case $H_J > H_{c1,\perp}$ is shown in Fig. 5. It describes correctly the limit of decoupled layers ($\rho = 0$), in which the tilted lattice cannot exist. In this limit, for $H_z < H_{c1,\perp}$, only the parallel lattice exists, while for

$H_z > H_{c1,\perp}$ we have the combined lattice (at $\rho = 0$, x-component of the field penetrates unperturbed whereas H_z results in perpendicular vortices).

D. High field regime

Let us consider now vortex lattices in high fields $H_a > H_0$ where 2D cores overlap. For the particular case of $\tan\theta = \gamma$ in the field $H_a = H_0$, the arrangement of singularities for tilted and perpendicular vortices is identical, see Fig. 6. The tilted vortex then is not a proper description for strong fields and high angles. We argue that in this case the combined lattice occurs. The energy of a parallel vortex is very small, and the energy of the parallel lattice in strong fields decreases with H_a as $(H_0/H_a)^2$.[10] Then, positions of singularities are determined mainly by electromagnetic coupling of 2D pancakes as in the model with zero Josephson coupling.[13,14] In this case the free energy reaches a minimum for the perpendicular arrangements of singularities (perpendicular vortices). Thus in strong fields and at high angles, the combined lattice is favorable irrespective of the ratio $H_J/H_{c1,\perp}$. The free energy for the parallel part of the lattice is obtained in Ref. 10, the energy of the perpendicular part is given by the standard London expression.

We conclude this section by noting that straight perpendicular vortices (pancakes arranged along the z direction) in the combined lattice are unstable with respect to small distortions caused by the Lorentz force induced by the in-plane currents of parallel vortices. A zigzag arrangement of pancakes in perpendicular vortices would have lower energy than the straight one; this effect determines mutual positions of parallel and perpendicular vortices, the subject to be discussed elsewhere.

VIII. MAGNETIC MOMENT AND TORQUE

The magnetization $\mathbf{M}$ and the torque density $\mathbf{T}$ are evaluated according to

$$\mathbf{M} = -\partial\tilde{G}/\partial\mathbf{H}_a, \quad \mathbf{T} = \mathbf{M} \times \mathbf{H}_a. \tag{8.1}$$

The component M_x is very small in fields $H \gg H_{c1}$ for systems of interest here; the essential quantity is M_z which gives $T_y = M_z H_{ax}$.

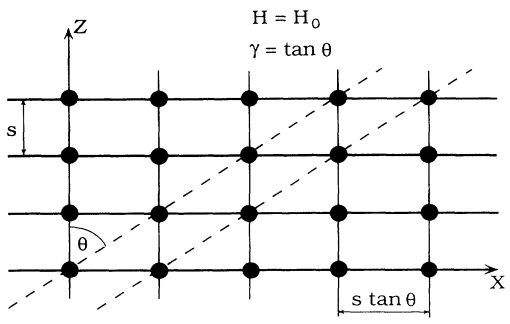

FIG. 6. Arrangement of phase singularities for the tilted (dashed lines) and perpendicular lattices (solid lines) in the field $H_a = H_0 = \phi_0/s^2\gamma$ at $\tan\theta = \gamma$.

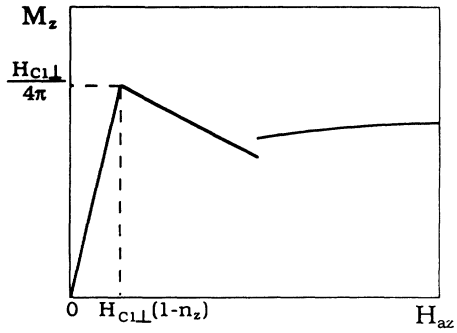

FIG. 7. The magnetization $|M_z|$ as a function of the z component of the applied field in the case of $H_J > H_{c1,\perp}$ and $(1 - n_z) \ll 1$.

For $H_J < H_{c1,\perp}$ (the phase diagram of Fig. 4), the component M_z has a broad maximum near $\tan\alpha \approx \gamma^{1/2}$. For $H_{az} \ll \gamma H_{ax}$ we obtain from Eqs. (6.10) and (7.1)

$$M_z = -\frac{\phi_0}{16\pi^2\lambda_{ab}^2}\left(\ln\frac{C_2C_4\lambda_J}{\xi_{ab}} + \frac{\gamma H_{az}}{2H_a}\ln\frac{H_0}{H_a}\right). \tag{8.2}$$

For $H_{az} \le H_{c1,\perp}$ vortices are locked in the parallel orientation. The system responds to the field H_{az} just as in the Meissner phase: $M_z = -H_{az}/4\pi$, see Fig. 4.

In the case $H_J > H_{c1,\perp}$ (the phase diagram of Fig. 5), with H_x increasing, when the first-order transition line is crossed, $|M_z|$ jumps to a lower value, the jump being of the order $\phi_0/16\pi^2\lambda_{ab}^2$. For the combined lattice, $|M_z|$ increases with angle α:

$$M_z = -\frac{\phi_0}{16\pi^2\lambda_{ab}^2}\ln\frac{\lambda_{ab}}{\xi_{ab}} + \frac{H_{az}}{4\pi} \tag{8.3}$$

until the lock-in transition, after which it drops linearly, see Fig. 7. For tilted and parallel lattices $|M_z|$ decreases with angle. This feature allows us to identify the combined lattice. Note that the H_{az} dependence of M_z for parallel and combined lattices is the same as for the Meissner state and the perpendicular vortex phase at $H_{ax} = 0$. This is because the parallel lattice can be considered as the Meissner state with respect to H_{az}, while in the combined lattice we have the system of perpendicular vortices which corresponds to a given H_{az}.

IX. DISCUSSION

Let us consider the question of validity of the 3D London and LD models for HTSC. The characteristic parameter $\rho_0 = 2\xi_{ab}^2(T = 0)/\gamma^2 s^2$ can be estimated using the perpendicular upper critical field H_{c2} (which gives ξ_{ab}), torque measurements (which give an accurate estimate of γ) and the structural data (which allow us to estimate s). In addition, the crossover temperature $T_{cr} = T_c(1 - \rho_0)$ provides direct information on the parameter ρ_0.

For $YBa_2Cu_3O_{7-x}$ according to the H_{c2} data,[35] $\xi_{ab} \approx 16$ Å and $\gamma \approx 5$. Torque measurements[20] on an untwinned sample yield $\gamma \approx 8$. This difference can be ex-

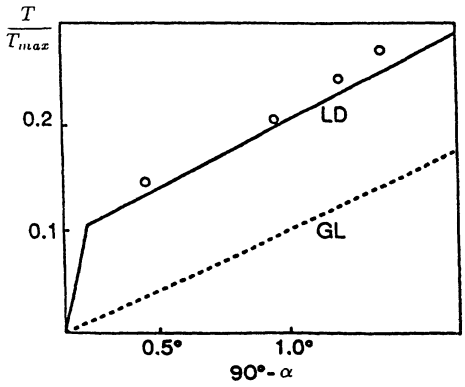

FIG. 8. Angular dependence of the torque at high angles for the Lawrence-Doniach and 3D anisotropic London models in the case $H_J < H_{c1,\perp}$. $T_{\max}$ is the maximum of the torque with respect to the angle. The circles are data for $YBa_2Cu_3O_7$ (Ref. 20).

plained by the strong dependence of γ on the oxygen content;[36] γ increases with x in the interval $0 < x < 0.1$ without a noticeable change of T_c. For $\gamma \approx 8$ and taking $s = 8$ Å (the distance between CuO_2 planes separated by a plane with CuO chains) we obtain $\rho_0 \approx 0.12$. High angle torque data for the sample with $\gamma \approx 8$ (Ref. 20) at $T = 75$ K and $H = 1$ T are shown in Fig. 8. Deviations from the 3D London predictions are seen clearly. They disappear above 80 K implying that the crossover temperature $T_{cr} \approx 80$ K. Using $T_c \approx 90$ K we obtain $\rho_0 \approx 0.12$ in accordance with the estimate made above. The torque data are in good agreement with the LD results, Eq. (8.2); the value of $\ln C_2$ obtained from this fit is ≈ -1.4, which compares well with -0.9 obtained within linear approximation. Thus, the LD model is able to explain the anomalous torque for $YBa_2Cu_3O_{7-x}$ assuming that phase diagram shown in Fig. 4 is valid for this material. For the lock-in critical angle $[\cot\alpha_c = (H_J/H_{ax})(1-n_z)]$ we obtain $2 \times 10^{-3}(1-n_z)$, i.e., the lock-in transition is practically absent in usually available platelet samples.

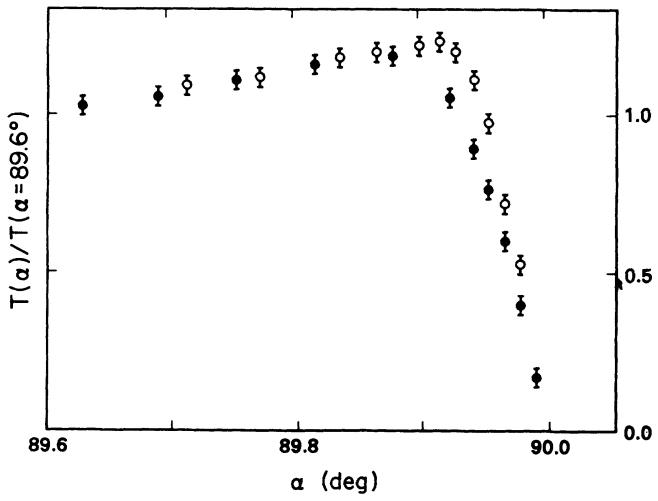

FIG. 9. Angular dependence of the torque $T(\alpha)/T(\alpha = 89.6°)$ of a single crystal $Tl_2Sr_2CaCu_2O_8$ at 90 K in the field $H_a = 7.7$ T (Ref. 21). Open circles correspond to the angle decreasing, and solid circles to the angle increasing.

For $Bi_2Sr_2CaCu_2O_8$ with approximately the same ξ_{ab} as in $YBa_2Cu_3O_{7-x}$ and with $\gamma \approx 55$,[20] the value ρ_0 is about 0.001; for $Tl_2Sr_2CaCu_2O_8$ with $\gamma \approx 500$,[37,38] ρ_0 is even smaller. Thus, these compounds are in the Josephson regime in a broad temperature interval. Figure 9 shows the torque data for $Tl_2Sr_2CaCu_2O_8$ with $T_c = 100$ K at $T = 90$ K and $H_a = 7.7$ T. The value H_0 for this compound is estimated as ≈ 4 T; this suggests that in the field of 8 T the tilted lattice does not exist. The sharp drop at $\theta = 89.92°$ can be attributed to the lock-in transition. The position of this drop agrees with the predicted value $H_{c1,\perp}(1-n_z)$ for $H_{c1,\perp} \approx 0.02$ T and $n_z \approx 0.5$ for the sample studied. An increase of the torque preceding the sharp drop can be taken as evidence for the combined lattice. There is a quantitative discrepancy between the predicted and measured values of the torque at the peak (the predicted value is approximately two times larger than the measured one). The discrepancy can be caused by sharp edges of the sample or by layers misalignment in the crystal studied. Such imperfections would smooth the peak value of the torque since the lock-in transition would have occurred at different angles in different parts of the sample.

We conclude by noting that the critical current is expected to change abruptly at the lock-in transition as well as at the transition combined-tilted lattices because the pinning should differ for parallel, tilted, and perpendicular vortices.

ACKNOWLEDGMENTS

The authors thank G. Blatter, J. R. Clem, D. Feinberg, V. B. Geshkenbein, and V. L. Pokrovskii for useful discussions and D. E. Farrell for providing experimental data prior to publication. Ames Laboratory is operated for the U.S. Department of Energy by Iowa State University under Contract No. W-7405-Eng-82. This research was supported by the Director for Energy Research, Office of Basic Energy Sciences, and in part through the Midwest Superconductivity Consortium, Grant No. DE-FG02-90ER45427. One of us (M.L.) acknowledges the support of the NSF Grant No. JF 898 under U.S.-Yugoslavia Cooperative Research Program.

APPENDIX A

The 3D anisotropic London equations for a vortex passing the origin along z_0 read[2]

$$h_i - \lambda^2 m_{kl}\varepsilon_{lsi}\varepsilon_{ktj}\frac{\partial^2 h_j}{\partial x_s \partial x_t} = \phi_0 \hat{z}_{0i}\delta(\mathbf{r}_0)\,. \qquad \text{(A1)}$$

Here ε_{ikl} is the unit antisymmetric tensor; $\lambda^2 m_{ik}$ is a tensor with eigenvalues $\lambda^2 m_a = \lambda_{ab}^2$ and $\lambda^2 m_c = \lambda_c^2$, such that $\lambda_{ab}^2\lambda_c = \lambda^3$, and $\mathbf{r}_0 = (x_0, y_0)$. Usually, these equations are written with z_0 as one of the coordinate axes, a justified choice because nothing depends on z_0 for a vortex in a uniform material. Within the LD scheme, this feature is lost anyhow, and the crystal itself represents

the most convenient frame. For the purpose of reference and comparison with LD results we describe here the 3D London vortex in this frame.

The crystal coordinates (x, y, z) (with z along the c axis) are obtained by rotation of (x_0, y_0, z_0) over the angle θ (the angle between the vortex axis and the c axis) round $\hat{\mathbf{y}}_0 = \hat{\mathbf{y}}$, which means: $\hat{\mathbf{z}}_0 = \hat{\mathbf{z}}\cos\theta + \hat{\mathbf{x}}\sin\theta$ and $\delta(\mathbf{r}_0) \equiv \delta(x_0)\delta(y_0) = \delta(x\cos\theta - z\sin\theta)\delta(y)$. Equations (A1) then yield

$$h_x - \lambda_{ab}^2\Delta h_x + (\lambda_c^2 - \lambda_{ab}^2)(4\pi/c)\nabla_y j_z = \phi_0 \sin\theta\, \delta(x\cos\theta - z\sin\theta)\delta(y),$$

$$h_y - \lambda_{ab}^2\Delta h_y + (\lambda_c^2 - \lambda_{ab}^2)(4\pi/c)\nabla_x j_z = 0, \tag{A2}$$

$$h_z - \lambda_{ab}^2\Delta h_z = \phi_0 \cos\theta\, \delta(x\cos\theta - z\sin\theta)\delta(y)\,.$$

Here $4\pi j_z/c = \mathrm{curl}_z \mathbf{h}$, and Δ is the 3D Laplacian. Note that, in fact, $\mathbf{h}(\mathbf{R})$ depends only on $(x - z\tan\theta)$ and y. The 2D Fourier transform (FT) of the field at $z = 0$ is

$$h_x = \phi_0 \tan\theta\,[1 + \lambda_{ab}^2(k_x^2\tan^2\theta + k_y^2) + \lambda_c^2 k_x^2]/d\,,$$

$$h_y = \phi_0 \tan\theta(\lambda_c^2 - \lambda_{ab}^2)k_x k_y/d\,, \tag{A3}$$

$$h_z = \phi_0/[1 + \lambda_{ab}^2(k_x^2\sec^2\theta + k_y^2)]\,,$$

where

$$d = [1 + \lambda_{ab}^2(k_x^2\sec^2\theta + k_y^2)](1 + \lambda_c^2 k^2 + \lambda_{ab}^2 k_x^2\tan^2\theta)\,.$$

Note that in the crystal frame, the equation for h_z is decoupled from others; $h_z(\mathbf{R})$ can be easily obtained either from the real space Eq. (A2) or from its Fourier transform (A3). This feature is preserved in the LD formalism; with the help of Eq. (2.4) we obtain

$$s\sum_n h_z(\mathbf{R})\delta(z - ns) - \lambda_{ab}^2\Delta h_z(\mathbf{R})\delta(z - ns) = \phi_0\delta(y)\sum_n \delta(x - na + a/2)\,. \tag{A4}$$

This equation can be solved with the help of FT, see Refs. 12 and 13.

The 2D Fourier solution for the current density is

$$j_x = i\phi_0 c k_y[1 + \lambda_c^2(k_x^2\sec^2\theta + k_y^2)]/4\pi d\,,$$

$$j_y = -i\phi_0 c k_x[1 + \lambda^2(\theta)(k_x^2\sec^2\theta + k_y^2)]/4\pi d\cos^2\theta\,, \tag{A5}$$

$$j_z = -i\phi_0 c k_y \tan\theta/4\pi(1 + \lambda_c^2 k^2 + \lambda_{ab}^2 k_x^2\tan^2\theta)\,,$$

where

$$\lambda^2(\theta) = \lambda_{ab}^2\sin^2\theta + \lambda_c^2\cos^2\theta\,. \tag{A6}$$

Within the LD model, in the linear approximation, the current $j_z(\mathbf{r}) = (c\phi_0/8\pi^2\lambda_c^2 s)\varphi \equiv j_0\varphi$. It is easy to check the same relation in the Fourier space: expand the rhs of (4.2) in $k_x a \ll 1$ and compare the result with $j_z(\mathbf{k})$ of the last equation (A5). In the real space formula (4.4), the 3D London limit corresponds to setting $\sin u = u$; this can be directly confirmed by integration over k_x in the inverse FT of $j_z(\mathbf{k})$.

From the last of Eqs. (A5) we find

$$j_z(\mathbf{r}) = \frac{\phi_0 c}{8\pi^2\lambda_{ab}\lambda_c^2}\frac{y}{r_1}K_1\left(\frac{r_1}{\lambda_c(1+\eta^2)^{1/2}}\right), \tag{A7}$$

$$\eta = \gamma\cot\theta\,, \quad r_1^2 = x^2\eta^2 + y^2(1+\eta^2)\,,$$

where K_1 is the modified Bessel function. The boundary of the region in the xy plane, where the London model differs substantially from the LD approach, can be estimated setting $|j_z(\mathbf{r})| = j_0$. The boundary is situated in the region where the argument of K_1 in (A7) is small; we then obtain

$$r_1^2 = |y|\lambda_J(1+\eta^2)^{1/2}\,. \tag{A8}$$

These are two identical ellipses touching each other at the origin and located symmetrically on opposite sides of the x axis. The width of the region enclosed by the curve in the x direction is $s\tan\theta$; in the y direction it is $2\lambda_J(1+\eta^2)^{-1/2}$.

The free energy per unit length of a London vortex has been obtained in Ref. 5:

$$\epsilon_L = \frac{\phi_0^2}{16\pi^2\lambda_{ab}^2}\left(\frac{\lambda(\theta)}{\lambda_c}\ln\frac{\lambda_c}{\xi_{ab}} + \cos\theta\ln\frac{\lambda_{ab}(1+\cos\theta)}{\lambda(\theta) + \lambda_c\cos\theta}\right). \tag{A9}$$

For large angles, $\tan\theta \gg \gamma$, the London line energy reads

$$\epsilon_L = \frac{\phi_0^2}{16\pi^2\lambda_{ab}\lambda_c}\left(\ln\frac{\lambda_c}{\xi_{ab}} + \frac{\gamma^2}{2\tan^2\theta}\ln\frac{\lambda_c C_{3L}}{\xi_{ab}}\right) \tag{A10}$$

with $C_{3L} = e^{-2} = 0.135$.

Taking the limit $\lambda_c \to \infty$, one obtains for $\theta \neq \pi/2$ the result of the model with pure electromagnetic coupling of the layers:[14]

$$\epsilon_{\mathrm{EM}} = \frac{\phi_0^2}{16\pi^2\lambda_{ab}^2}\cos\theta\ln\frac{\lambda_{ab}(1+\cos\theta)}{2\xi_{ab}\cos\theta}\,. \tag{A11}$$

The free energy of the equilibrium vortex lattice in intermediate fields, $H_{c1} \ll H \ll H_{c2}$, reads (see Ref. 5) in our notation

$$F = \frac{B^2}{8\pi} + \frac{\phi_0(B_x^2 + \gamma^2 B_z^2)^{1/2}}{32\pi^2\lambda_{ab}\lambda_c}\ln\frac{\gamma H_{c2,\perp}C_1'}{(B_x^2 + \gamma^2 B_z^2)^{1/2}}, \tag{A12}$$

where the parameter C_1' on the order unity depends on the lattice structure. The leading term in the potential $\tilde{G}$ of Eq. (7.1) is $(F - B^2/8\pi)$. Thus, for the tilted lattice

$$\tilde{G}_t = \frac{\phi_0(B_x^2 + \gamma^2 B_z^2)^{1/2}}{32\pi^2\lambda_{ab}\lambda_c}\ln\frac{\gamma H_{c2,\perp}C_1'}{(B_x^2 + \gamma^2 B_z^2)^{1/2}}\,. \tag{A13}$$

For the combined lattice of perpendicular and parallel London vortices we have $\tilde{G}_c = \tilde{G}_\perp + \tilde{G}_\parallel$ with

$$\tilde{G}_\perp = \frac{\phi_0 B_z}{32\pi^2\lambda_{ab}^2} \ln \frac{H_{c2,\perp} C_1'}{B_z},$$

$$\tilde{G}_\parallel = \frac{\phi_0 B_x}{32\pi^2\lambda_{ab}\lambda_c} \ln \frac{\gamma H_{c2,\perp} C_1'}{B_x}. \tag{A14}$$

The tilted London lattice is always preferable to the combined one: use the inequality $(B_x^2 + \gamma^2 B_z^2)^{1/2} < B_x + \gamma B_z$ in the prelogarithm factor of $\tilde{G}_t$ to show that $\tilde{G}_t - (\tilde{G}_\perp + \tilde{G}_\parallel)$ is always negative.

APPENDIX B

In Fourier representation Eqs. (2.4) read

$$(k_y^2 + q^2) A_x(\mathbf{k}, q) - k_x k_y A_y(\mathbf{k}, q) = -\frac{s}{\lambda_{ab}^2}\left(\tilde{A}_x(\mathbf{k}, q) + \frac{\phi_0}{2\pi}\Phi_x(\mathbf{k}, q)\right) \tag{B1}$$

with another equation obtained from (B1) by the interchange $x \leftrightarrow y$. Here

$$A_\alpha(\mathbf{k}, q) = \int d\mathbf{r}\, dz\, A_\alpha(\mathbf{r}, z) \exp[-i(\mathbf{kr} + qz)],$$

$$\tilde{A}_\alpha(\mathbf{k}, q) = \sum_n \int d\mathbf{r}\, dz\, A_\alpha(\mathbf{r}, z)\delta(z - ns) \exp[-i(\mathbf{kr} + qz)],$$

$$\Phi_\alpha(\mathbf{k}, q) = \sum_n \int d\mathbf{r}\, dz\, \Phi_{n,\alpha}(\mathbf{r})\delta(z - ns) \exp[-i(\mathbf{kr} + qz)], \quad \Phi_{n,\alpha}(\mathbf{r}) = \nabla_\alpha \Phi_n(\mathbf{r}),$$

with $\alpha = x, y$. Denoting the rhs of (B1) by $-a_\alpha$ we have

$$A_x(\mathbf{k}, q) = \frac{a_x(k_x^2 + q^2) + a_y k_x k_y}{q^2(k^2 + q^2)}; \tag{B2}$$

to obtain an equation for A_y, interchange x and y.

Using the definition of $\tilde{A}_\alpha$ one can prove[13] the relation

$$\tilde{A}_\alpha(\mathbf{k}, q) = \frac{1}{s}\sum_m A_\alpha\left(\mathbf{k}, q + \frac{2\pi m}{s}\right), \tag{B3}$$

which verifies that $\tilde{A}_\alpha(\mathbf{k}, q)$ is periodic in q with period $2\pi/s$. With the help of this property we obtain from Eq. (B2)

$$\tilde{A}_x(\mathbf{k}, q) = \frac{a_x}{s}\sum_m \frac{k_x^2 + q_m^2}{q_m^2(k^2 + q_m^2)} + \frac{a_y}{s} k_x k_y \sum_m \frac{1}{q_m^2(k^2 + q_m^2)}, \tag{B4}$$

where $q_m = q + 2\pi m/s$. An equation for $\tilde{A}_y(\mathbf{k}, q)$ is obtained after $x \leftrightarrow y$. Solving these two linear equations for $\tilde{A}_x(\mathbf{k}, q)$ and $\tilde{A}_y(\mathbf{k}, q)$ yields

$$\tilde{A}_x(\mathbf{k}, q) = -\frac{\phi_0}{2\pi} \frac{\Phi_x(\mathbf{k}, q)[k_x^2 \Lambda_{0q} + k_y^2 \Lambda_{kq} + k^2 \Lambda_{0q}\Lambda_{kq}] + \Phi_y(\mathbf{k}, q) k_x k_y (\Lambda_{0q} - \Lambda_{kq})}{k^2(1 + \Lambda_{0q})(1 + \Lambda_{kq})}, \tag{B5}$$

and a similar expression for $\tilde{A}_y(\mathbf{k}, q)$ ($x \leftrightarrow y$), where

$$\lambda_{ab}^2 \Lambda_{kq} = \sum_m \frac{1}{k^2 + q_m^2} = \frac{s}{2k} \frac{\sinh(ks)}{\cosh(ks) - \cos(qs)}. \tag{B6}$$

Also, one can verify that

$$k_x \tilde{A}_x(\mathbf{k}, q) + k_y \tilde{A}_y(\mathbf{k}, q) = -\frac{\phi_0}{2\pi} \frac{\Lambda_{0q}}{1 + \Lambda_{0q}} [k_x \Phi_x(\mathbf{k}, q) + k_y \Phi_y(\mathbf{k}, q)]. \tag{B7}$$

Now we use the relation $\varphi_{n,n+1}(\mathbf{r}) = \Phi_n(\mathbf{r}) - \Phi_{n+1}(\mathbf{r})$ and Eq. (3.4) to obtain $\Phi_x(\mathbf{k}, q)$ and $\Phi_y(\mathbf{k}, q)$ in terms of $\varphi_{\mathbf{k}}$:

$$2\Phi_x(\mathbf{k}, q) \sin\frac{k_x a}{2} = k_x \varphi_{\mathbf{k}} \delta(qs + k_x a),$$

$$2\Phi_y(\mathbf{k}, q) \sin\frac{k_x a}{2} = \left(k_y \varphi_{\mathbf{k}} - \frac{4\pi i}{k_x} \sin\frac{k_x a}{2}\right) \delta(qs + k_x a). \tag{B8}$$

Then, with the help of Eq. (2.11), we find $j_{n\mathbf{k}}$ in terms of $\varphi_{\mathbf{k}}$. Inserting the phases Φ into (B5) and using Eqs. (2.11), (2.14), and (3.5) we obtain Eq. (3.7).

Since $ks < s/\xi_{ab} \ll 1$, we can use in the free-energy calculation

$$\lambda_{ab}^2 \Lambda_{kq} \approx \frac{s^2}{4\sin^2(qs/2) + k^2 s^2}. \tag{B9}$$

APPENDIX C

Consider an integral

$$I = \frac{1}{2\pi\beta} \int_{x^2+y^2 \le R^2} \frac{dx\,dy}{1 + x^2 + y^2\beta^{-2}}, \tag{C1}$$

where $R \gg 1$. Asymptotically,

$$I = \ln \frac{2R}{1+\beta}. \tag{C2}$$

Integration over an infinite strip parallel to x gives

$$\frac{1}{2\pi\beta} \int_{-R}^{R} dy \int_{-\infty}^{\infty} \frac{dx}{1 + x^2 + y^2\beta^{-2}} = \ln \frac{2R}{\beta}. \tag{C3}$$

On the other hand,

$$\frac{1}{2\pi\beta} \int_{-R}^{R} dx \int_{-\infty}^{\infty} \frac{dy}{1 + x^2 + y^2\beta^{-2}} = \ln(2R). \tag{C4}$$

We see that for $\beta \ll 1$ the procedure (C4) gives a correct answer. For $\beta \gg 1$ the procedure (C3) should be used, if we are to evaluate the integral with logarithmic accuracy for large or small values of β. Thus, one can replace the circular region of integration by an infinite strip parallel to the direction of the fastest decrease of the integrand.

The difference between (C3) and (C4) is $\ln\beta$. In the domain of angles $\tan\theta \gg \gamma$ the parameter $\beta = \gamma/\tan\theta$ according to Eq. (5.2); this gives an extra factor in logarithm in the third term of Eq. (6.1). In the domain of angles $\tan\theta \ll \gamma$ the factor $\beta = 1 + \tan\theta/\gamma$, and the difference between (C3) and (C4) is negligible.

*Permanent address: Institute of Physics, P.O. Box 57, 11001 Belgrade, Yugoslavia.

[1] V. L. Ginzburg, Zh. Eksp. Teor. Fiz. **14**, 134 (1944).

[2] V. Kogan, Phys. Rev. B **24**, 1572 (1981).

[3] A. V. Balatskii, L. I. Burlachkov, and L. P. Gor'kov, Zh. Eksp. Teor. Fiz. **90**, 1478 (1986) [Sov. Phys. JETP **63**, 866 (1986)].

[4] A. M. Grishin, A. Yu. Martynovich, and S. V. Yampolskii, Zh. Eksp. Teor. Fiz. **97**, 1930 (1990) [Sov. Phys. JETP **70**, 1089 (1990)].

[5] V. G. Kogan, N. Nakagawa, and S. L. Thiemann, Phys. Rev. B **42**, 2631 (1990); L. J. Campbell, M. M. Doria, and V. G. Kogan, *ibid.* **38**, 2439 (1988).

[6] W. E. Lawrence and S. Doniach, in *Proceedings of 12th International Conference on Low Temperature Physics, Kyoto 1970*, edited by E. Kanda (Keigaku, Tokyo, 1970), p. 361.

[7] R. Klemm, M. R. Beasley, and A. Luther, J. Low Temp. Phys. **16**, 607 (1974).

[8] L. N. Bulaevskii, Zh. Eksp. Teor. Fiz. **64**, 2241 (1973) [Sov. Phys. JETP **37**, 1143 (1973)].

[9] J. R. Clem and M. W. Coffey, Phys. Rev. B **42**, 6209 (1990); J. R. Clem, M. W. Coffey, and Z. Hao, *ibid.* **44**, 2732 (1991).

[10] L. N. Bulaevskii and J. R. Clem, Phys. Rev. B **44**, 10 234 (1991).

[11] I. O. Kulik and I. K. Yanson, *The Josephson Effect in Superconducting Tunneling Structures* (Israel Program for Scientific Translation, Jerusalem, 1972).

[12] K. B. Efetov, Zh. Eksp. Teor. Fiz. **76**, 1781 (1979) [Sov. Phys. JETP **49**, 905 (1979)].

[13] A. Buzdin and D. Feinberg, J. Phys. (Paris) **51**, 1971 (1990).

[14] J. R. Clem, Phys. Rev. B **43**, 7837 (1991).

[15] S. Doniach, in *High Temperature Superconductivity, Los Alamos Symposium, 1989*, edited by K. S. Bedel *et al.* (Addison-Wesley, Redwood City, 1990), p. 406. The value λ_J introduced as γs coincides with the Josephson length in the junction made of thin films if their thickness is much smaller than the penetration depth, see Ref. 11.

[16] S. Ryu, S. Doniach, G. Deutscher, and A. Kapitulnik, Phys. Rev. Lett. **68**, 710 (1992).

[17] D. Feinberg and C. Villard, Phys. Rev. Lett. **65**, 919 (1990).

[18] B. I. Ivlev, Y. N. Ovchinnikov, and V. L. Pokrovskii, Mod. Phys. Lett. **5**, 73 (1991). The term F_1 in the free energy should be dropped according to the authors (private communication).

[19] L. Fruchter and I. A. Campbell, Phys. Rev. B **40**, 5158 (1989).

[20] D. E. Farrell, J. P. Rice, D. M. Ginsberg, and J. Z. Liu, Phys. Rev. Lett. **64**, 1573 (1990).

[21] R. G. Beck, M. F. Booth, D. E. Farrell, J. P. Rice, and D. M. Ginsberg (unpublished).

[22] V. G. Kogan, Phys. Rev. B **38**, 7049 (1988).

[23] P. H. Kes, J. Aarts, V. M. Vinokur, and C. J. van der Beek, Phys. Rev. Lett. **64**, 1063 (1990).

[24] S. Theodorakis, Phys. Rev. B **42**, 10 172 (1990).

[25] S. N. Artemenko and A. N. Kruglov, Physica C **173**, 125 (1991).

[26] A. A. Abrikosov, *Fundamentals of the Theory of Metals* (North-Holland, Amsterdam, 1988).

[27] V. Cataudella and P. Minnhagen, Physica C **166**, 442 (1990).

[28] D. Feinberg (unpublished).

[29] J. R. Clem, Proceedings of the 6th International Workshop on Critical Currents, 1991 (IOP Publishing, Bristol).

[30] J. L. Harden and V. Arp, Cryogenics **3**, 30 (1963); J. R. Clem, J. Low Temp. Phys. **18**, 427 (1975).

[31] L. N. Bulaevskii, Phys. Rev. B **44**, 910 (1990).

[32] S. S. Maslov and V. L. Pokrovsky, Pis'ma Zh. Eksp. Teor. Fiz. **53**, 614 (1991) [JETP Lett. **53**, 637 (1991)].

[33] L. D. Landau and E. M. Lifshitz, *Electrodynamics of the Continuous Media* (Pergamon, Oxford, 1983).

[34] R. A. Klemm and J. R. Clem, Phys. Rev. B **21**, 1868 (1980).

[35] U. Welp, W. K. Kwok, G. W. Crabtree, K. G. Vandervoort, and J. Z. Liu, Phys. Rev. Lett. **62**, 1908 (1989).

[36] B. Janoossi, D. Prost, S. Pekker, and L. Fruchter, Physica C **181**, 51 (1991).

[37] K. E. Grey, R. T. Kampwirth, and D. E. Farrell, Phys. Rev. B **41**, 819 (1990).

[38] D. E. Farrell, R. G. Beck, M. F. Booth, C. J. Allen, E. D. Bukowski, and D. M. Ginsberg, Phys. Rev. B **42**, 6758 (1990).